

**Low-energy photoelectron dynamics in Kr  $3d_{5/2}$  photoionization followed by Auger decay**

Qianxia Wang and S. D. Loch\*

*Department of Physics, Auburn University, Alabama 36849, USA*

(Received 10 April 2015; published 19 May 2015)

The effects induced during the process of inner-shell photoionization followed by Auger decay are investigated for the photoionization of Kr  $3d_{5/2}$  in an extremely low photoelectron energy regime. Both the photoelectron energy and relative angular distributions are calculated with a recently developed quantum-mechanical method where all the Coulomb interactions between each pair of particles are fully considered. The photoelectron energy distribution is asymmetric with respect to the initial photoelectron energy, and its peak shifts to a lower energy. As the absorbed photon energy is reduced, the peak of the photoelectron energy distribution moves to the negative energy range. As a manifestation of these dynamics, peak structures are observed in the relative angular distribution. We also simulate the process with a classical-trajectory Monte Carlo method, obtaining similar results to the quantum-mechanical ones.

DOI: [10.1103/PhysRevA.91.053416](https://doi.org/10.1103/PhysRevA.91.053416)

PACS number(s): 32.80.Fb, 32.80.Hd

**I. INTRODUCTION**

The physical process of photoabsorption followed by sequential double ionization has been studied extensively in the past decades [1–17]. The first electron emitted from the nucleus is called the photoelectron because its ionization is due to photoabsorption. If the photoelectron originates from an inner shell, a second electron may undergo an Auger decay and be emitted (referred to as the Auger electron). How quickly the photoelectron and Auger electron escape from the atom and the period between the two ionizations are two important factors in determining the subsequent dynamics. The initial energy of the Auger electron  $E_2$  and the Auger width  $\Gamma$  (proportional to the inverse of the time interval between the two ionizations) depend upon only the chosen atomic system. The initial photoelectron energy  $E_1$  is a function of the incident photon energy and the ionization potential of the ionizing electron. In summary, the atomic species and the incident photon energy codetermine the whole physical process.

During the past decades, this problem has been investigated within different atomic systems, namely,  $4d_{3/2,5/2}$  photoionization following  $N-OO$  Auger decay in Xe [1–7], Ar  $3d$  photoionization followed by Auger decay [12,13],  $1s$  or  $2s$  photoionization with subsequent Auger decay in Ne [8–11,17], and  $3d_{5/2,3/2}$  photoionization followed by Auger decay in Kr [15,16]. These papers covered a wide energy range. Xe is one of the most frequently used atom species in studying this problem. The  $4d_{5/2}$  photoionization in xenon with subsequent  $N_5-O_{2,3}O_{2,3}$  Auger decay was selected to study the energy and/or angular distributions in Refs. [1–7]. For this system, the initial energy of the Auger electron  $E_2$  was  $\sim 30$  eV, and the Auger width  $\Gamma$  was  $\sim 0.12$  eV. The initial photoelectron energy  $E_1$  was  $E_p - 67.548$  eV, with a variable  $E_p$  ( $E_p$  is the incident photon energy, and 67.548 eV is the binding energy of  $4d_{5/2}$  [18]).  $E_1$  was 27 eV in [1,2], where the influences of the postcollision interaction (PCI) on the energy and angular distributions for a particular ejection angular range were studied.  $E_1$  was 30.0 eV in the work of Viefhaus *et al.* [3]; they showed that the triple differential cross section can fully vanish because of destructive interference. Scherer

*et al.* [4] considered the energy distribution measurement of two coincident electrons with nearly the same energy and direction, and three different initial photoelectron energies, 28.97, 29.97, and 30.97 eV, were studied. The first coincident angular distribution was measured in Ref. [6], where  $E_1$  was 29.9 eV. Sheinerman *et al.* experimentally and theoretically investigated the PCI phenomena with the same atomic system in Ref. [7], and the initial photoelectron energy was as low as 2.67 eV. In the same reference, other Xe systems, such as  $4d_{3/2}$  photoionization with subsequent decays  $N_4-O_{2,3}O_{2,3}$  and  $N_4-O_1O_{2,3}$ , were also included in their investigations, where  $E_2$  was  $\sim 32$  and 16 eV, respectively, the energy for  $4d_{3/2}$  was  $-69.537$  eV, and  $\Gamma$  was  $\sim 0.104$  eV for the intermediate state.

Inner-shell photoionization followed by Auger decay is a three-body problem and cannot be solved exactly in an analytical way. However, some approximations can be made to convert it to a two-body problem if neither of the two electrons have low energies. If the energy of one of the two electrons is low, for example,  $E_1$  is very low and the Auger electron is ejected with a high velocity, the interaction between the ion and photoelectron has to be fully considered during the whole process. In this situation, this problem can also be solved analytically by approximately treating the  $e-e$  interaction and the interaction between the Auger electron and ion. Different cases with low initial photoelectron energy have been investigated in Refs. [8,12,13,15,16]. Because the  $e-e$  interaction was not fully considered, only the energy distribution was calculated, and the angular distribution was rarely involved. The main purpose of this paper is to investigate how the angular distribution behaves when the photoelectron is emitted with extremely low energy.

To achieve this goal, we perform calculations with a numerical method [17,19,20] and refer to this as the time-dependent Schrödinger equation (TDSE) method in which all Coulomb interactions between each pair of particles are fully taken into account. To confirm the validity of the results, we also redo the calculations with a classical-trajectory Monte Carlo (CTMC) method. The chosen system in this paper is Kr  $3d_{5/2}$  photoionization with subsequent  $M-NN$  Auger decay, and the photoelectron energy is between 0.0 and 1.0 eV. We select this system because it has small  $\Gamma$  ( $\sim 0.088$  eV) and lower  $E_2$  ( $\sim 2$  a.u.), which are within the limitations of the TDSE method; see the discussion in Sec. II.

\*loch@physics.auburn.edu

This paper is organized as follows: in Sec. II, we briefly review the two theoretical methods used in this paper, TDSE and CTMC; Sec. III shows the energy and angular distributions for the system Kr  $4d_{5/2}$  photoionization following  $M$ - $NN$  Auger decay. The last section presents the conclusion.

Atomic units are used throughout unless stated otherwise.

## II. THEORETICAL METHODS

### A. Quantum-mechanical method

The whole process can be divided into two steps, before and after the Auger decay. For the quantum-mechanical method [17,19,20] used in this paper, we use Eq. (1), a time-independent inhomogeneous equation, to describe the propagation of the photoelectron; the process after the Auger decay is described by a time-dependent Schrödinger equation with a source term for the two ionized electrons [Eq. (2)]. By solving the two equations, we can obtain the two-electron wave function in real time [ $\Lambda(\mathbf{r}_1, \mathbf{r}_2, t)$ ], from which different physical quantities can be extracted.

The time-independent inhomogeneous equation for the process before the Auger decay is

$$\left(E_1 + i\frac{\Gamma}{2} - H_\alpha\right) F_1 = D\phi_g, \quad (1)$$

where  $D\phi_g$  describes photon absorption of the electron,  $F_1$  is the photoelectron wave function,  $H_\alpha$  is the Hamiltonian of the photoelectron before the Auger decay, and  $\Gamma$  is the width of the inner vacancy. The potential in  $H_\alpha$  is taken as  $-1/r$ ,  $D\phi_g$  is taken to be a simple short-range function, and  $\Gamma$  is proportional to the inverse of the inner vacancy's lifetime.

The time-dependent Schrödinger equation for the process after the Auger decay is

$$i\frac{\partial \Lambda}{\partial t} - H\Lambda = S(t)F_1(r_1)F_2(r_2), \quad (2)$$

where  $S(t)$  is the strength of the source,  $F_2(r_2)$  is the source term for the Auger electron, and  $H$  is the total Hamiltonian. We use  $S(t) = 1/[1 + \exp\{10(1 - 5t/t_f)\}]$ , where  $t_f$  is the final time of the calculation [17]. There are three parts in  $H$ : the Hamiltonian for the photoelectron, the Auger electron, and the interaction between the two ionized electrons. The potential for the photoelectron and Auger electron is taken to be  $-2/r$  because the ion is doubly charged after the Auger decay.

The two-electron wave function  $\Lambda$  can be expressed as

$$\Lambda = \sum_{\ell_1, \ell_2} R_{\ell_1 \ell_2}^{\text{LS}}(r_1, r_2, t) \sum_{m_1, m_2} C_{m_1 m_2 0}^{\ell_1 \ell_2 L} Y_{\ell_1 m_1}(\Omega_1) Y_{\ell_2 m_2}(\Omega_2), \quad (3)$$

where  $C_{m_1 m_2 m_3}^{\ell_1 \ell_2 \ell_3}$  is a Clebsch-Gordan coefficient,  $\Omega$  is the solid angle, and  $Y_{\ell m}(\Omega)$  is a spherical harmonic. We assume that the two electrons have zero total angular momentum ( $L = 0$ ), and the two electrons have the same angular momentum ( $\ell_1 = \ell_2 = \ell$ ). Then Eq. (3) is simplified as

$$\Lambda = \sum_{\ell} \frac{(-1)^{\ell}}{\sqrt{4\pi}} R_{\ell}(r_1, r_2, t) Y_{\ell 0}(\cos \theta_{12}), \quad (4)$$

where  $Y_{\ell 0}(\cos \theta_{12})$  is a spherical harmonic and  $\theta_{12}$  is the relative angle between the two ionized electrons.

The method to extract the photoelectron energy and angular distributions [ $P_{\epsilon_1}$  and  $D_k(\cos \theta_{12})$ ] with the total wave function  $\Lambda$  was shown in Ref. [20]. One point that deserves emphasis is that the angular distribution  $D_k$  counts only electrons with positive energies, and those that are captured to the bound states during the Auger process are excluded. Below we describe how to calculate two other physical quantities [the angular and photoelectron energy distribution (PED) and the angular momentum distribution for those ionized photoelectrons  $P_{\ell}$ ], which will also be used in the next section.

One quantity is the PED which is a probability distribution for the photoelectron energy and relative angle. It can be calculated via

$$A_{\ell}(\epsilon_1, \epsilon_2) = \iint dr_1 dr_2 \phi_{\epsilon_1 \ell}^*(r_1) \phi_{\epsilon_2 \ell}^*(r_2) R_{\ell}(r_1, r_2, t) \quad (5)$$

and

$$\text{PED} = \int d\epsilon_2 \left| \sum_{\ell=0}^{\ell_{\max}} (-1)^{\ell} Y_{\ell 0}^*(\cos \theta_{12}) A_{\ell}(\epsilon_1, \epsilon_2) \right|^2, \quad (6)$$

where 1 and 2 correspond to the photoelectron and Auger electron, respectively,  $\epsilon_{1,2}$  is positive energy, and  $\phi_{\epsilon_{1,2}\ell}(r_{1,2})$  is the eigen wave function for the continuum electron; for the photoelectron, the continuum wave is for a potential  $-2/r$ , while for the Auger electron the potential is  $-1/r$ .

The other quantity is the angular momentum distribution for the ionized photoelectrons  $P_{\ell}$ , which can be calculated via

$$P_{\ell} = \int d\epsilon_2 \int d\epsilon_1 |A_{\ell}(\epsilon_1, \epsilon_2)|^2. \quad (7)$$

Last, we discuss the approximations used in the TDSE method. Our results are insensitive to different expressions for the short-range functions  $D\phi_g$  and  $F_2$ .  $-Z/r$  is the potential we use in the Hamiltonians. The correlation with other electrons cannot be neglected when the photoelectron or Auger electron travels close to the nucleus. We redid our calculations with the expression  $-[Z + (Z_t - Z)\exp(-r/r_a)]/r$  for the potential instead ( $r_a$  and  $Z_t$  are the atomic radius and number, respectively,  $r_a = 1.66$  a.u. and  $Z_t = 36$  for Kr). Compared with the previous results, there are only small changes in the angular distributions for cases  $E_1 = 0.0$  and  $0.1$  eV and almost no changes for other cases in this paper. We also suppose that both emitted electrons start with zero angular momentum. During the subsequent electron dynamics, the two electrons have the same angular momentum magnitude because the total angular momentum (which is zero) is conserved. Due to the expected complexity, we did not perform calculations for other total angular momentum values. This approximation is expected to work well in the chosen system. The small Auger width means that the photoelectron has a longer time to travel away from the nucleus before the Auger decay. Meanwhile, the initial Auger electron energy is not high, which postpones the strongest interaction between the photoelectron and Auger electron. The validity of the zero total angular momentum approximation will be increased if the two electrons meet far away from the nucleus. Moreover, we focus on those electrons that remain ionized from the ion, which makes this approximation more accurate.

### B. Classical-trajectory Monte Carlo method

The TDSE method described above has been proven to be valid in studying inner-shell photoionization followed by Auger decay problems [17,20]. However, we apply this method to the extremely low photoelectron energy region, which is of particular interest for the scenarios studied here, where the calculated angular distributions have unusual shapes. Thus it is desirable to check the results with a completely different theoretical method. We simulate the process with a CTMC approach [19].

In our classical simulation, the photoelectron is emitted from the nucleus at  $t = 0$ , with a random energy selected from a normal distribution  $\exp[-(E - E_1)^2/2\sigma^2]$ , where  $E_1$  is the initial photoelectron energy used in the quantum-mechanical method and  $\sigma$  equals  $\Gamma/2\sqrt{2\ln 2}$ , with a random direction chosen from flat  $\cos \theta$  and flat  $\phi$ ; the Auger electron is launched at  $t = t_2$ , where  $t_2$  is chosen from an exponential distribution  $\Gamma \exp(-\Gamma t)$ , with a random energy selected from a normal distribution  $\exp[-(E - E_2)^2/2\sigma^2]$ , where  $E_2$  is the initial Auger electron energy used in the TDSE method, with a fixed direction  $\theta = \pi/2$  and  $\phi = 0$ . Note that we make the two electrons propagate from a small radius (0.001 a.u.) to avoid the infinite Coulomb potential and velocity at the starting point, and the two electrons' positions are updated using Newton's second law until the relative angle distribution does not change. The relative angle between the two electrons  $\theta_{12}$  is calculated via  $\cos \theta_{12} = \frac{v_1 \cdot v_2}{v_1 v_2}$ .

### III. RESULTS AND DISCUSSION

The system chosen in this paper is Kr  $3d_{5/2}$  photoionization followed by  $M-NN$  Auger decay, where  $\Gamma$  is  $\sim 0.088$  eV and  $E_2$  is  $\sim 2$  a.u. We will study the photoelectron energy and angular distributions in this system by changing the photon energy. The cases included in this paper are  $E_1 = 1.0, 0.5, 0.25, 0.125, 0.1$ , and  $0.0$  eV. We first investigate in Sec. III A the changes to the photoelectron energy distributions, and then in Sec. III B we consider the changes to the relative angular distributions.

#### A. The photoelectron energy distribution

Figure 1 displays the photoelectron energy distribution after the Auger decay for different initial photoelectron energies. Figure 1(a) is for cases  $E_1 = 1.0$  eV (dot-dashed line),  $0.5$  eV (dotted line),  $0.25$  eV (dashed line),  $0.125$  eV (thin solid line), and  $0.1$  eV (thick solid line); Fig. 1(b) is for the case  $E_1 = 0.0$  eV, which needs a greater energy range to show the complete distribution. For each case, the energy of the photoelectron might be expected to be symmetrically centered on the initial photoelectron energy  $E_1$  before the Auger decay [9]. After the Auger decay, the maximum of the distribution is shifted to smaller energy, and the distribution becomes asymmetric. As shown in Fig. 1(a), the shift of the distribution peak is  $\delta E = 1.0 - 0.88 = 0.12$  eV for the case  $E_1 = 1.0$  eV,  $\delta E = 0.5 - 0.33 = 0.17$  eV for the case  $E_1 = 0.5$  eV, and  $\delta E = 0.25 - 0.05 = 0.2$  eV for the case  $E_1 = 0.25$  eV. The peaks for the other three cases are shifted to the negative energy region; their shifts cannot be calculated here.

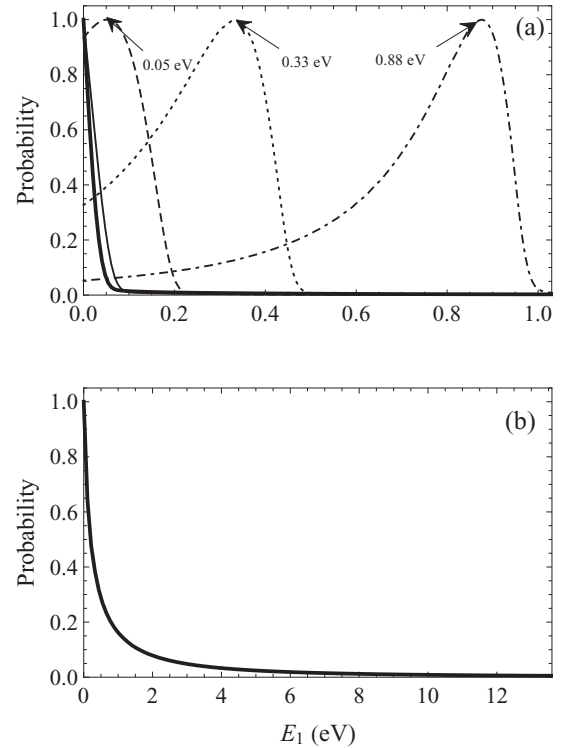


FIG. 1. The photoelectron energy distributions (normalized by dividing by the maximum probability in positive energy range) for cases (a)  $E_1 = 1.0$  eV (dot-dashed line),  $0.5$  eV (dotted line),  $0.25$  eV (dashed line),  $0.125$  eV (thin solid line), and  $0.1$  eV (thick solid line) and (b)  $E_1 = 0.0$  eV (thick solid line). The arrows point to the energy with maximum probability, which is  $0.88$  eV for the case  $E_1 = 1.0$  eV,  $0.33$  eV for the case  $E_1 = 0.5$  eV, and  $0.05$  eV for the case  $E_1 = 0.25$  eV.

This phenomenon is caused mainly by the abrupt change in the ion's charge when the Auger decay happens. The increase in the ion charge reduces the ion potential by  $1/r_0$ , where  $r_0$  is the distance the photoelectron travels away from the nucleus before the Auger electron is launched. Cases with larger initial photoelectron energy have smaller shifts of the distribution peak because the lifetime of the intermediate state is approximately the same for each case and the larger initial photoelectron energy causes larger  $r_0$ . Within the same case, the shift in energy of  $1/r_0$  is smaller if the photoelectron has larger energy, which can explain why the energy distribution is broader and asymmetric and why the tail of the left side of the distribution lasts longer than that of the right side.

The interaction between the photoelectron and Auger electron also has some influence on the shift of the energy distribution. The Auger electron will transfer part of its energy to the photoelectron when it passes by. The stronger the interaction is, the more energy the photoelectron will obtain. We have performed calculations for some cases with the same initial photoelectron energy and Auger width but different initial Auger energies. The shifts of the distribution peak  $\delta E$  are not the same, although the energy shifts caused by the change of the ion charge would be expected to be the same. The reason is that their  $e-e$  interaction strengths are different. Lower initial Auger energy means that the Auger electron can

interact with the photoelectron for a longer time; more energy will be transferred to the photoelectron energy, which makes the shift  $\delta E$  smaller.

Figures 1(a) and 1(b) also show that a small portion of photoelectrons are captured to bound states after the Auger decay if the photoelectron has a relatively high initial energy  $E_1$ ; however, when  $E_1$  becomes smaller, more and more photoelectrons will stay at bound states. We expect that the angular distribution profiles of cases  $E_1 = 1.0$  and  $0.5$  eV will be determined by the strength of the interaction between the photoelectron and Auger electron and have a normal profile, while the captured photoelectrons will seriously distort the angular distributions of the other four cases.

### B. The angular distribution discussion

The electron-electron interaction is usually considered the main factor in determining the shape of the relative angular distribution. When the two ionized electrons travel in the same direction, the fast Auger electron will push the slow photoelectron away by a small relative angle and will pass by. Thus in the angular distribution, the probability at  $\cos\theta_{12} = 1$  is much lower than that of the other relative angular positions, and the probability at a small nonzero relative angle is higher. If the two ionized electrons travel with a larger relative angle, they do not interact significantly with each other, making the distribution flat at those angular positions. As shown in Fig. 2, the curves for cases  $E_1 = 1.0$  eV (dot-dashed line) and  $0.5$  eV (dotted line) have the overall features stated above. The strength of the interaction will change the depth of the hole at  $\cos\theta_{12} = 1$  and the height of the convexity nearby. This is not the focus of this paper. Instead, we investigate the effects from those captured photoelectrons, which affect the shape of the angular distribution when  $E_1$  is extremely low.

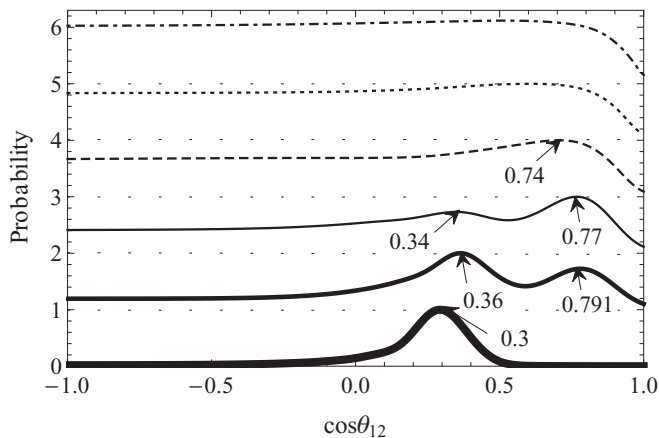


FIG. 2. The angular probability distributions calculated by the TDSE method (normalized by dividing by the maximum probability) for cases  $E_1 = 1.0$  eV (dot-dashed line, shifted up by 5.0),  $0.5$  eV (dotted line, shifted up by 4.0),  $0.25$  eV (dashed line, shifted up by 3.0),  $0.125$  eV (thin solid line, shifted up by 2.0),  $0.1$  eV (medium solid line, shifted up by 1.0), and  $0.0$  eV (thick solid line). The arrows point to the angular positions of peak(s), which are  $\cos\theta_{12} = 0.74$  for the case  $E_1 = 0.25$  eV,  $\cos\theta_{12} = 0.34$  and  $0.77$  for the case  $E_1 = 0.125$  eV,  $\cos\theta_{12} = 0.36$  and  $0.791$  for the case  $E_1 = 0.1$  eV, and  $\cos\theta_{12} = 0.3$  for the case  $E_1 = 0.0$  eV.

Next, we investigate how the capture of the photoelectrons reshapes the angular distribution. We refer to this factor as the capture factor below. As shown in Fig. 1, more and more photoelectrons are captured by the ion as one decreases the initial photoelectron energy. Correspondingly, the angular distributions (shown in Fig. 2) are distorted by the capture factor to varying degrees. The influence of this factor on the angular distribution appears as a sharpening of the curve at the angular position with the highest probability or in the creation of a nearby peak. This phenomenon happens because the angular distributions shown in Fig. 2 count only the photoelectrons with positive energy and exclude those captured by the nucleus which are distributed unevenly over the relative angular position. The photoelectrons at the angular position with the highest distribution probability are usually more energetic because they have strongly interacted with the Auger electron and have gained more energy. They are unlikely to be captured to the nucleus, and the possibility for photoelectrons at other angular position of being captured is high, which results in one or two sharper peaks at the angular distribution.

We analyze the angular distributions displayed in Fig. 2 in more detail. For the case  $E_1 = 1.0$  eV (dot-dashed line), almost no photoelectrons are captured by the nucleus. Its angular distribution has the expected shape. A small part of the photoelectrons is captured for the case  $E_1 = 0.5$  eV (dotted line). The capture factor exerts little influence on the angular distribution, and the shape is close to a standard one. When the initial photoelectron energy decreases to  $E_1 = 0.25$  eV (dashed line), the angular distribution has a sharp peak in the angular position near zero relative angle. The capture factor starts to play an important role in the angular distribution shape. For cases  $E_1 = 0.125$  eV (thin solid line),  $0.1$  eV (medium solid line), and  $0.0$  eV (thick solid line), most photoelectrons do not have enough energy to ionize. Their angular distributions show that the probability of a large range of angular position is low because only a small portion of the photoelectrons escapes the capture of the nucleus and these electrons are largely centered around the peak of the distribution. For cases  $E_1 = 0.125$  and  $0.1$  eV, the successfully ionized photoelectrons come from two sources: one part (component 1) is those with positive energy at the momentum when the Auger decay happens, and the other part (component 2) is those with negative energy when the Auger decay happens that gain enough energy for ionization from the Auger electron while being passed. These two components of the ionized photoelectrons correspond to the two peaks in their angular distributions. The left peak in the angular distribution is for component 2, and the right one is for component 1. The reason for this conclusion is as follows. Those photoelectrons with negative energy at first will interact with the Auger electron at a small radius, and they can be pushed to a larger relative angular position. However, for the photoelectrons with positive energy at first, the strongest  $e-e$  interaction happens at a larger radius, and the interaction will disappear when the photoelectrons are pushed to a small relative angle because the distance between the two electrons is large. We believe the two sources also exist in cases  $E_1 = 0.25$  and  $0.0$  eV, but only one peak appears in their angular distributions because the numbers of ionized photoelectrons from the two sources are not comparable. Component 1 dominates among the ionized photoelectrons for the case  $E_1 = 0.25$  eV, and most ionized

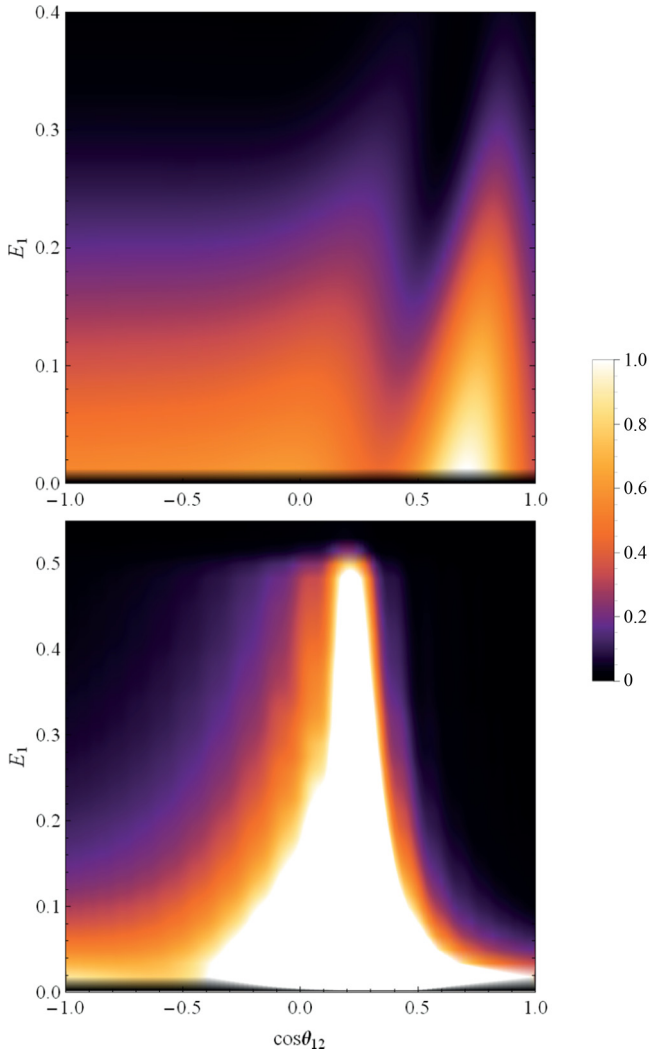


FIG. 3. (Color online) The physical quantity PED for cases (top)  $E_1 = 0.125$  eV and (bottom) 0.0 eV.

photoelectrons come from component 2 for the case  $E_2 = 0.0$  eV.

Two physical quantities may be helpful in demonstrating the explanations above. One is the PED, which displays the distribution of the photoelectron energy and relative angle, and the other is the angular momentum distribution for those ionized photoelectrons  $P_\ell$ . We show PED for two cases in Fig. 3; the top panel is for the case  $E_1 = 0.125$  eV, and the bottom panel is for the case  $E_1 = 0.0$  eV. The color indicates the size of the probability. There are two bright spots in the plot for the case  $E_1 = 0.125$  eV and one bright spot for the case  $E_1 = 0.0$  eV, which correspond to two peaks or one peak in their angular distributions shown in Fig. 2. The main purpose of this plot is to demonstrate that the photoelectrons with higher energy are centered on the peak area for which the capture factor plays an important role in reshaping the angular distribution.

Figure 4 shows the angular momentum distributions for the ionized photoelectrons of different cases, which include  $E_1 = 1.0$  eV (red dot-dashed line), 0.5 eV (green dotted line), 0.25 eV (blue dashed line), 0.125 eV (thin solid line), 0.1 eV (medium solid line), and 0.0 eV (thick solid line),

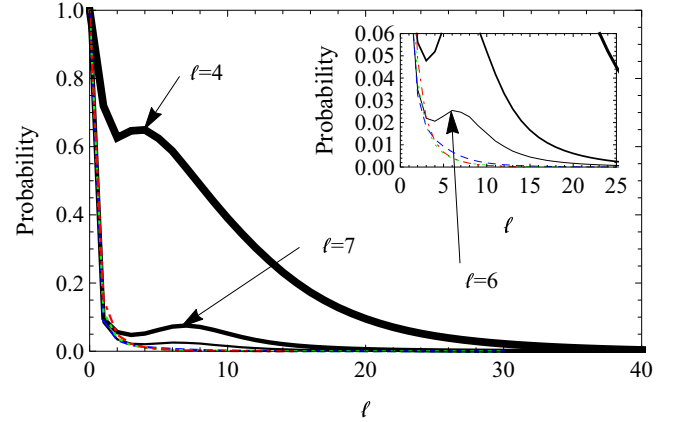


FIG. 4. (Color online) The angular momentum distributions for the ionized photoelectrons (normalized by dividing by the maximum probability) of cases  $E_1 = 1.0$  eV (red dot-dashed line), 0.5 eV (green dotted line), 0.25 eV (blue dashed line), 0.125 eV (thin solid line), 0.1 eV (medium solid line), and 0.0 eV (thick solid line). The arrows point to the angular momentum positions of the second peak, which are  $\ell = 6$  for the case  $E_1 = 0.125$  eV,  $\ell = 7$  for the case  $E_1 = 0.1$  eV, and  $\ell = 4$  for the case  $E_1 = 0.0$  eV.

0.1 eV (medium solid line), and 0.0 eV (thick solid line). For all of the cases, the maximum probability in each angular momentum distribution is at  $\ell = 0$ . This phenomenon is reasonable because we assume that the photoelectron starts with zero angular momentum and its angular momentum remains the same during the following time propagation, except for interacting with the Auger electron when both particles are emitted in a similar direction. Figure 4 also shows that the proportion of the ionized photoelectrons with high angular momentum is larger in the low  $E_1$  cases, which demonstrates our explanation for the unusual shape in the angular distribution. For the cases with very low  $E_1$ , a large part of those photoelectrons that successfully escape from the nucleus is due to the strong interaction with the Auger electron, which leads to the phenomenon that more ionized electrons are distributed at higher angular momenta. In the angular momentum distribution, there is a second peak for cases  $E_1 = 0.0, 0.1,$  and  $0.125$  eV. The peak position is at  $\ell = 4$  for the case  $E_1 = 0.0$  eV,  $\ell = 7$  for the case  $E_1 = 0.1$  eV, and  $\ell = 6$  for the case  $E_1 = 0.125$  eV. There is no regularity for the position of the second peak, but we can conclude that cases with lower  $E_1$  have a sharper second peak.

We simulate the whole process with a completely different theory, the classical-trajectory Monte Carlo method. Figure 5 displays the angular distributions for cases  $E_1 = 1.0$  eV (dot-dashed line), 0.5 eV (dotted line), 0.25 eV (dashed line), 0.125 eV (thin solid line), 0.1 eV (medium solid line), and 0.0 eV (thick solid line). The main differences between Figs. 5 and 2 lie in two points. One is that the probability at  $\cos \theta_{12} = 1$  is not exactly zero in Fig. 2 for cases with nonzero initial photoelectron energy; however, it is very close to zero in Fig. 5. This difference comes from the different descriptions of particles in quantum and classical mechanics. In quantum mechanics, electrons are also waves which make it possible for the two ionized electrons to move in the same direction,

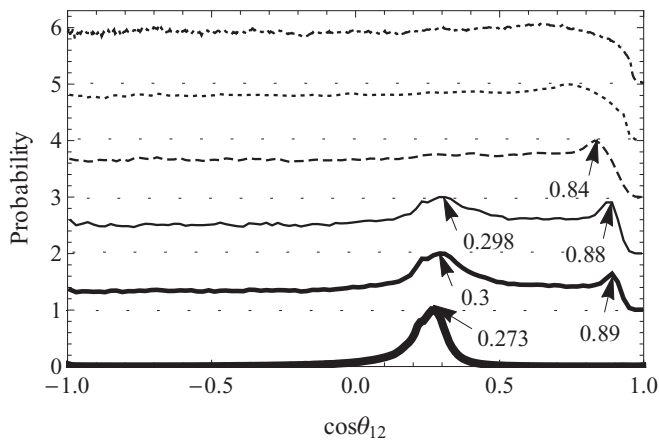


FIG. 5. The angular probability distributions calculated by the CTMC method (normalized by dividing by the maximum probability) for cases  $E_1 = 1.0$  eV (dot-dashed line, shifted up by 5.0), 0.5 eV (dotted line, shifted up by 4.0), 0.25 eV (dashed line, shifted up by 3.0), 0.125 eV (thin solid line, shifted up by 2.0), 0.1 eV (medium solid line, shifted up by 1.0), and 0.0 eV (thick solid line). The arrows point to the angular positions of the peak(s), which are  $\cos \theta_{12} = 0.84$  for the case  $E_1 = 0.25$  eV,  $\cos \theta_{12} = 0.298$  and  $0.88$  for the case  $E_1 = 0.125$  eV,  $\cos \theta_{12} = 0.3$  and  $0.89$  for the case  $E_1 = 0.1$  eV, and  $\cos \theta_{12} = 0.273$  for the case  $E_1 = 0.0$  eV.

while in classical mechanics the photoelectron has to be pushed aside and then the Auger electron can pass by. The other point is that the angular positions of the peaks are slightly different and the relative heights of the two peaks for the case  $E_1 = 0.125$  eV are different. A possible explanation is that the captured photoelectrons move in an elliptical orbit in quantum mechanics, while in our classical theory they oscillate along the radius.

There are two points that are worthy of note. One is that the situation with two peaks in the angular distribution does not always happen. We did not find cases with two

peaks in the angular distribution if they have a large  $\Gamma$ . A possible reason is that the ionized photoelectrons from the two sources are not separated far enough for the short traveling time before the Auger decay, and components 1 and 2 of the ionized photoelectrons mix together. The other point is that the calculations performed in this paper do not consider reemission of those nonionized photoelectrons, which may happen during the experiment because the ion may be left at an excited state and could transfer energy to the captured photoelectrons to make them ionize. In order to obtain the angular distribution with similar features shown in Fig. 2, those reemitted photoelectrons have to be excluded.

#### IV. CONCLUSIONS

We investigated the scenario of photoionization followed by Auger decay in the extremely low photoelectron energy region. The system chosen was Kr  $3d_{5/2}$  photoionization followed by  $M-NN$  Auger decay in which  $\Gamma$  is  $\sim 0.088$  eV and  $E_2$  is  $\sim 2$  a.u.. We have performed calculations of the energy and angular distributions for cases  $E_1 = 1.0, 0.5, 0.25, 0.125, 0.1,$  and  $0.0$  eV. The energy distribution shifts to smaller energies because of the abrupt decrease in the ion potential. The shift becomes larger when the initial photoelectron energy is decreased. For the angular distribution, the capture factor plays an increasingly important role in the shape of the distribution with the decrease of the initial photoelectron energy, with a peaked profile being predicted for very low energy cases.

#### ACKNOWLEDGMENTS

We are grateful to Dr. F. Robicheaux for the idea for this paper. Thanks go to Dr. C. P. Ballance for his assistance during writing the code for the CTMC method. We also thank Dr. A. Landers for very useful feedback on our results. Finally, we would like to thank B. Yang, S. Wang, and R. Koch for a critical reading of the manuscript.

- 
- [1] B. Kämmerling, B. Krässig, and V. Schmidt, *J. Phys. B* **26**, 261 (1993).
  - [2] M. Yu. Kuchiev and S. A. Sheinerman, *J. Phys. B* **27**, 2943 (1994).
  - [3] J. Viehhaus, G. Snell, R. Hentges, M. Wiedenhöft, F. Heiser, O. Geßner, and U. Becker, *Phys. Rev. Lett.* **80**, 1618 (1998).
  - [4] N. Scherer, H. Lörch, T. Kerkau, and V. Schmidt, *Phys. Rev. Lett.* **82**, 4615 (1999).
  - [5] N. Scherer, H. Lörch, T. Kerkau, and V. Schmidt, *J. Phys. B* **37**, L121 (2004).
  - [6] M. Wiedenhoef, S. E. Canton, A. A. Wills, T. Gorczyca, J. Viehhaus, U. Becker, and N. Berrah, *J. Phys. B* **41**, 095202 (2008).
  - [7] S. Sheinerman, P. Lablanquie, F. Penent, J. Palaudoux, J. H. D. Eland, T. Aoto, Y. Hikosaka, and K. Ito, *J. Phys. B* **39**, 1017 (2006).
  - [8] S. A. Sheinerman, *J. Phys. B* **38**, 2279 (2005).
  - [9] A. L. Landers *et al.*, *Phys. Rev. Lett.* **102**, 223001 (2009).
  - [10] S. Rioual, B. Rouvellou, L. Avaldi, G. Battera, R. Camilloni, G. Stefani, and G. Turri, *Phys. Rev. Lett.* **86**, 1470 (2001).
  - [11] B. Rouvellou, S. Rioual, L. Avaldi, R. Camilloni, G. Stefani, and G. Turri, *Phys. Rev. A* **67**, 012706 (2003).
  - [12] M. Yu. Kuchiev and S. A. Sheinerman, *J. Phys. B* **21**, 2027 (1988).
  - [13] P. Bolognesi, A. De Fanis, M. Coreno, and L. Avaldi, *Phys. Rev. A* **70**, 022701 (2004).
  - [14] S. A. Sheinerman and V. Schmidt, *J. Phys. B* **30**, 1677 (1997).
  - [15] S. Sheinerman, P. Lablanquie, and F. Penent, *J. Phys. B* **40**, 1889 (2007).
  - [16] F. Penent, S. Sheinerman, L. Andric, P. Lablanquie *et al.*, *J. Phys. B* **41**, 045002 (2008).
  - [17] F. Robicheaux, M. P. Jones, M. Schoffler *et al.*, *J. Phys. B* **45**, 175001 (2012).
  - [18] V. Schmidt, *Electron Spectrometry of Atoms Using Synchrotron Radiation* (Cambridge University Press, Cambridge, 1997), pp. 275–276.
  - [19] F. Robicheaux, *J. Phys. B* **45**, 135007 (2012).
  - [20] Q. Wang, S. Sheinerman, and F. Robicheaux, *J. Phys. B* **47**, 215003 (2014).